

Stochastic Geometry Analysis of Sojourn Time in RF/VLC Hybrid Networks

Rabe Arshad and Lutz Lampe

Abstract—The spectrum scarcity in the radio frequency (RF) communication in indoor environments motivates the integration of an alternative technology like visible light communication (VLC) with the existing RF architecture that results in a hybrid RF/VLC network. While VLC helps offloading the congested RF spectrum by offering capacity-per-area improvements, the resulting heterogeneity and narrow coverage areas of optical base stations (BSs) impose several challenges for user mobility such as unnecessary handovers. To help addressing these challenges, in this paper, we derive the mean and the distribution of sojourn time in RF/VLC hybrid networks. The mathematical analysis conducted in this paper makes use of the tools from stochastic geometry and abstracting the BSs' locations via two independent homogeneous Poisson point processes (PPPs). Since PPP modeling is yet to be well established for RF/VLC hybrid networks, we compare the PPP based analytical results to those obtained for an actual deployment, a Matérn hard-core point process (MHCPP) based deployment, and a deterministic square lattice deployment of VLC luminaries. Furthermore, we utilize the sojourn time distribution to calculate the unnecessary handover probability. Our numerical results show the interplay between the sojourn time and the receiver field of view as a function of BS density and they highlight the cost of BS densification in terms of unnecessary handovers.

Index Terms—Association probabilities, Hybrid networks, Radio frequency networks, Sojourn time, Stochastic geometry, Visible light communication

I. INTRODUCTION

The next generation wireless networks are expected to offer high data rates and ultra-low latency connectivity. This is being realized via an extreme phase of network densification and the integration of new technologies such as visible light communication (VLC) with the existing radio frequency (RF) infrastructure especially in indoor environments that hold around 80% of the overall mobile traffic [1]. The resulting hybrid RF/VLC network combines the benefits of two technologies and thus offers higher data rates and tackles the limitations of individual technologies like link blockages in VLC only networks and congested spectrum issues in RF only networks [2]. In fact, it has been demonstrated in [3] that a hybrid RF/VLC network offers a total throughput greater than that of a stand-alone VLC or RF network.

The hybrid RF/VLC network has recently gained much attention from the academia and the industry. Several studies including [4]–[6] are available in the literature that motivate the use of a hybrid RF/VLC network. Several case studies have

also been conducted where a hybrid architecture is deployed in both academic and industrial environments [7]. Although the aforementioned studies motivated the deployment of a hybrid network, there exist some other studies that focus on its performance analyses. For instance, the authors in [8] studied and optimized the energy efficiency in hybrid RF/VLC networks. The authors in [9] minimized the transmit power consumption in the hybrid network while achieving the required quality of service. The coverage and the rate analysis in hybrid RF/VLC networks was conducted in [10]. The authors in [11] optimized the radio base stations (RBSs) and optical base stations (OBSs) intensities to minimize the area power consumption under the outage probability constraint. The authors in [12] studied an energy-efficient resource management in the context of industrial networks to guarantee the diverse requirements of internet of things devices. An optimal resource allocation scheme was presented in [13] to maximize the corresponding data rate by assuming a common backhaul network. The authors in [14] studied the effective capacity in a hybrid RF/VLC network in the presence of an eavesdropper. The aforementioned studies focussed on the energy, resources, and rate performance for stationary users in a hybrid network and hence the user mobility aspect was not addressed.

While the hybrid RF/VLC networks are able to offer several benefits including better coverage, capacity, and localization accuracy, the increased network densification and heterogeneity impose several challenges for the user mobility. The reduced per-BS coverage areas in a hybrid RF/VLC network encourage mobile users to perform frequent changes in the user-to-BS association, which may incur unnecessary delays and an additional signalling overhead. Thus, it is crucial to study the mobility-aware performance metrics as they can directly impact the service experience of the mobile users. In this context, relevant mobility aware performance metrics include handover rate, handover probability, and sojourn time [15]. Handover rate is defined as the ratio of the average number of cells a mobile user traverses to the average transition time [16]. Handover rate is used to determine the ping pong handover rate, handover failure rate, quantify the mobility effect into the signalling overhead, power consumption, and average throughput experienced by the user [17]–[21]. On the other hand, handover probability is defined as the probability that the user performs a handover in one movement period [22]. Handover probability is used to investigate the handover drop probability and unnecessary handover probability [23]. Note that under certain conditions (e.g., low user velocity),

the handover rate is equal to the handover probability [15]. Sojourn time or cell dwell time, which is the time duration that a mobile user resides within a typical cell, is a key performance metric that can help studying other important performance metrics like channel holding time, HO drop probability, and unnecessary HO probability. Thus, an accurate analysis of mobility-aware performance metrics is necessary to design, optimize, and assess the performance of wireless networks.

A. Related Work

In the context of user mobility management and relevant mobility aware performance metrics, several studies exist in the literature for RF only networks. For instance, the authors in [16], [22], [24], [25] used different approaches to characterize HO rates and probabilities in Poisson point process (PPP) based single/multi-tier RF networks. In [16], the authors proposed a tractable random waypoint (RWP) mobility model to analyze the handover rates in a single tier RF network. The authors in [24] used an arbitrary movement trajectory to characterize the handover rates in multi-tier heterogeneous wireless networks. While the authors in [16] and [24] used a trajectory based approach to characterize handover rates, the authors in [22] used an association based approach to characterize handover probability. Although [22] considered a multi-tier RF network, the analytical framework was presented for horizontal handovers only (i.e., intra-tier handovers). The authors in [25] used an association based approach to characterize horizontal and vertical handover probabilities in a multi-tier heterogeneous wireless network. Further, the handover rate modeling in [24] was extended in [26] with a general path-loss exponent and in [27] to compute HO rates in three-dimensional multi-tier RF networks. Recently, using an equivalence distance approach, the authors in [28] studied handover probability in hybrid RF and terahertz wireless network. Furthermore, several articles including [29]–[33] studied HO related algorithms and management techniques to reduce the unnecessary HOs and improve the user experience in RF only networks. In the context of sojourn time analysis, the authors in [16] characterized mean sojourn time and its distribution in a single tier RF network. In [34], the mean sojourn time was approximately derived where multiple small cells were irregularly deployed within each macro cell. The authors in [35] derived the mean sojourn time in the small cells of a two tier cellular network. Moreover, modeling BSs' locations via independent PPPs, [36] characterized mean sojourn time and its distribution in a multi-tier RF network. In [36], the authors showed that the handover rate is inversely proportional to the sojourn time. Also, the complementary cumulative distribution function of sojourn time is upper bounded by the complement of the handover probability. However, the existing sojourn time characterization models presented in the literature (i.e., [16], [34]–[36]) cannot directly be applied to VLC networks due to the involvement of the VLC centric elements like field-of-view (FOV) of VLC receivers where the handover boundaries of the OBSs depend on the receiver FOV. For standalone VLC networks, the authors in [37]

derived HO rate and HO probability by taking receiver rotation into account. The authors in [38]–[40] presented HO related algorithms to enhance the overall user experience. The authors in [41] studied mean sojourn time in a single tier VLC network. Recently, the authors in [42] studied sojourn time and ping-pong HO rate in a multi-tier VLC network. Relatively fewer studies exist for hybrid RF/VLC networks that tackle the user mobility issues and analyze the mobility-aware performance metrics. For instance, the authors in [3] studied the handover effects on load balancing in a hybrid RF/VLC network. The authors in [43] discussed different mechanisms to mitigate the frequent handover issues in hybrid RF/VLC networks. Recently, the authors in [44] characterized HO rates under two different user-to-BS association policies in a hybrid RF/VLC setting. However, the sojourn time analysis in a hybrid RF/VLC network is still an open problem.

The significance of sojourn time analysis emanates from the dependency of several important network key performance indicators (KPIs) including channel holding time, HO failure rate, and ping-pong (or unnecessary) HO rate on the sojourn time [36]. Channel holding time is defined as the time duration for which a user communicates with one cell. Having the information about channel holding time helps planning the cell capacity and traffic offloading between different network tiers [45]. Further, a HO failure occurs when the sojourn time in the target cell is less than the HO execution time [46]. Moreover, a HO is considered to be unnecessary if the sojourn time in the new cell is less than a predefined threshold. Hence, reducing the HO failure and ping-pong HO rates alleviates service disruptions and improves the quality of service experienced by mobile users. Note that the user mobility analysis becomes more crucial in denser networks due to narrow BSs' coverage footprints resulting in frequent HOs. This is the main motivation for us to study the sojourn time in RF/VLC hybrid networks.

For a general study on the user mobility aware performance metrics, a random BS deployment is usually considered. This stems from the fact that the mobility aware performance metrics are largely impacted by the BSs' locations and the network density. To capture the impact of network densification on the network performance, stochastic geometry aided mathematical analyses are well accepted in the literature. Stochastic geometry is a mathematical tool that helps modeling the randomness in BSs's locations via different point processes and calculates the spatial averages of the performance metrics. Among different point processes, PPP is widely adopted due to its simplicity, tractability, and the performance closer to that of an actual wireless network [24], [47]. Although PPP is well established in case of RF, some recent studies on RF/VLC hybrid networks have abstracted BSs' locations via PPP to study coverage and HO rates [10], [44]. Also, it is shown in [44] that the PPP modeling offers similar HO rates when compared to the actual RF/VLC deployment. However, a stochastic geometry aided sojourn time analysis and a performance comparison with respect to an actual deployment

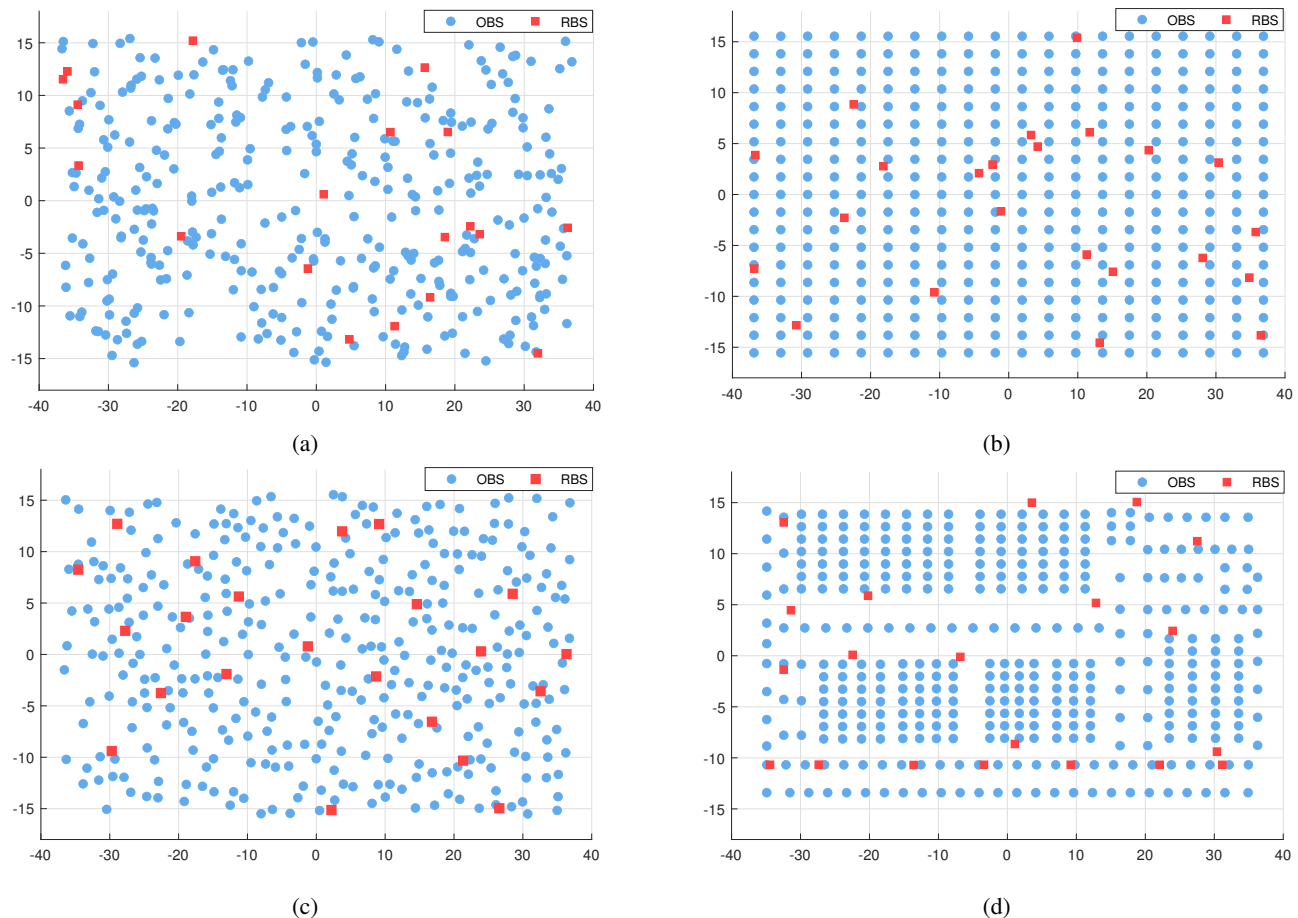


Fig. 1: A two tier RF and optical BS network in a 74 m × 31 m indoor area according to four deployment models: (a) PPP, (b) square lattice deployment for VLC and PPP for RF, (c) Matérn HCPCP with inter-BS distance thresholds $d_v = 1.3$ m, $d_r = 5$ m, (d) an actual deployment in a university building. OBSs and RBSs are represented by blue circles and red squares, respectively.

scenario are yet to be conducted for RF/VLC hybrid networks.

B. Paper Contributions

The key contributions of this paper are summarized as follows.

- We derive the linear contact and chord length distributions to mathematically express the mean and the distribution of sojourn time in RF/VLC hybrid networks. In the context of VLC networks, the existing works compute the sojourn time in a single tier network where the cells are convex. Due to disparity in the transmission powers of RBSs and OBSs in a hybrid network, the cells may not be convex, which complicates the analysis. For the analytical model, we exploit the stochastic geometry tools and abstract the BSs' locations via PPP and validate the results via Monte-Carlo simulations.
- The PPP modeling is necessary to mathematically characterize the sojourn time¹. Although, PPP approximation

¹The non-PPP models are mathematically less tractable to derive the contact distance function and the nearest neighbor function. This is due to the fact that the points are not independent in non-PPP models. Hence, it is more appropriate to use a PPP model, which favors mathematical tractability and provides meaningful insights on the system design [48].

- is well established for RF based studies, it has not been fully evaluated in case of VLC. For instance, the existing luminaries deployment may call for a more regular deployment like a square lattice or a hard-core point process (HCPCP) approximation, however, the wiring complexities and uncertain lighting requirements in some areas may result in a more random-like deployment [49]. Thus, in order to conduct a more comprehensive study, we use simulations to model the BSs' locations via square lattice and Matérn HCPCP (MHCPCP) in addition to the PPP and compare the results from an actual deployment of luminaries in a university building. All the deployment scenarios considered in this study are shown in Fig. 1. We compare the mean sojourn time for the different deployment scenarios and motivate the applicability of PPP through results from an actual deployment setting.
- Using the developed mathematical model, we study unnecessary HO probability and investigate the impact of an VLC centric element (i.e. receiver FOV) on the HO performance. Moreover, via simulation results from the actual deployment scenario, it is shown that the developed mathematical model captures the user mobility perfor-

TABLE I: Mathematical Notations

| Notation | Description |
|-------------------|--|
| λ_k | BS intensity of k^{th} tier |
| P_T | Transmit power of RBSs |
| P_{elec} | Electrical transmit power of OBSs |
| P_{opt} | Optical transmit power of OBSs |
| B_k | Bias factor of k^{th} tier |
| h_k | Height of k^{th} tier BS |
| Z_k | Euclidean distance between the user and the nearest k^{th} tier BS |
| R_k | Horizontal distance between the user and the nearest k^{th} tier BS |
| η | Free space path-loss exponent |
| n_c | Optical-to-electrical conversion ratio |
| ψ | Angle of incidence from nearest OBS to the user |
| \bar{S} | Sojourn time in the cell where the connection was initiated |
| G | DC channel gain for VLC communication |
| v | User Velocity |
| ζ | Receiver field-of-view |
| B, C | RF Propagation model dependent constants |
| A_k | Probability of associating to the k^{th} tier BS |
| S | Sojourn time |

mance in RF/VLC hybrid networks.

One of the major challenges in this study lies in the complexity of the analytical modeling, which is due to the involvement of different path loss models, BSs' heights, and receiver FOV. Hence, the presented solutions for the mean and the distribution of sojourn time are not closed form but require numerical integration over some parameters.

C. Paper Organization and Notations

The rest of the paper is organized as follows. The system model is presented in Section II. The mathematical framework is discussed in Section III. Finally, the simulation setup and the performance comparison among different deployment strategies are discussed in Section IV followed by the conclusion in Section V. The mathematical notations used in the paper are summarized in Table I.

II. HYBRID RF/VLC SYSTEM MODEL

In this section, we describe the system model for the RF/VLC hybrid network.

A. Network Model

Consider a two tier hybrid RF/VLC network and let $\mathcal{K} = \{r, v\}$, where "r" and "v" represent RBSs and OBSs, respectively. The BSs' locations in the two tier RF/VLC hybrid network are abstracted via four different deployment models as shown in Fig. 1. In the PPP scenario, the number of BSs inside any bounded region follows a Poisson distribution and the BSs are randomly located within the defined area. The BSs belonging to the k^{th} tier, where $k \in \mathcal{K}$ have an intensity λ_k and are placed via a two-dimensional homogeneous PPP Φ_k at height h_k . In the square lattice deployment scenario, the VLC and RF BSs' locations are modeled via a grid pattern and a

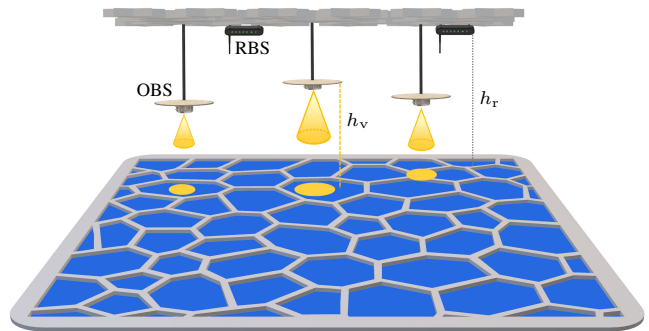


Fig. 2: A two tier RF/VLC hybrid network with a sample Voronoi tessellation. The RBS and the OBS coverage areas are represented by blue and yellow colors, respectively. For a clear illustration, only few RBSs are shown in the figure.

PPP, respectively, where the total numbers of BSs are obtained from the actual lighting and Wi-Fi BSs data in accordance with the actual deployment case. MHCPP deployment is achieved from a dependent thinning applied to a homogeneous PPP such that the inter-BS distance d_k is not less than a pre-defined threshold [50]. Finally, the actual deployment is obtained from the lighting and Wi-Fi BSs arrangements on a building floor at the University of British Columbia. The mean sojourn time and its distribution are mathematically derived for PPP but are computed via simulations for other deployment models. For all deployment models, the RBSs and the OBSs are assumed to be located at the ceiling and are oriented vertically downward. There exists no blockage between the user and the serving BS and hence, the link failures do not occur. Without loss of generality, we conduct our analysis on a test mobile user that follows a random waypoint mobility model and moves with a fixed velocity v . The test user is equipped with both RF and VLC receivers. The VLC receiver uses a photo-detector that is assumed to face toward the ceiling, which is in accordance with the recent studies [10], [44], [51].

The user-to-BS association in the two tier RF/VLC hybrid network follows the maximum biased received signal strength (RSS) association policy. Thus, the user associates to the BS that offers the best received signal strength. This association policy has been studied in [47], [52] for RF, in [41] for VLC, and in [10], [44] for hybrid RF/VLC networks. It is assumed that all triggered HOs are successful and no HO failure occurs due to resource unavailability. Under the RSS policy, the coverage areas of the RBSs and the OBSs can be visualized via a weighted Voronoi tessellation [53], which is illustrated in Fig. 2.

B. Channel Model

The WINNER channel model is considered for RF communication as it is widely accepted for indoor networks [54]. Using the WINNER channel model, the received power can be modeled as $P^{\text{RF}} = P_T X Z_r^{-\eta}$, where P_T denotes the RBS transmit power, Z_r represents the Euclidean distance between the user and the nearest RBS, η is the free space path-loss exponent, and $X = 10^{-\frac{\gamma}{10}}$, $\gamma = B + C \log_{10}(f_c/5)$,

f_c represents the carrier frequency in GHz, and B and C are propagation model dependent constants. For the line-of-sight (LOS) communication, the typical values of propagation model dependent constants are $B = 46.3$ and $C = 20$ [54].

The received power from an OBS is modeled as $P^{\text{VLC}} = P_{\text{elec}} G^2 R_{\text{pd}}^2$, where P_{elec} denotes the electrical transmit power, G represents the VLC channel gain, and R_{pd} is the responsivity of the photo-detector in the receiver [55]. The average electrical and the optical power in direct current biased optical orthogonal frequency division multiplexing system are related by $P_{\text{elec}} = P_{\text{opt}}^2/n_c^2$, where n_c is the optical-to-electrical conversion ratio [56]. Due to high intensity of OBSs, there exists a high probability of having the LOS communication between the OBS and the user. Thus, the LOS direct current (DC) channel gain is used in the analysis, which is modeled via the Lambertian emission model and is given by [57]

$$G = \begin{cases} \frac{A_{\text{pd}}(m+1)}{2\pi Z_v^2} \cos^m(\phi) \cos(\psi) G(\zeta) T(\zeta), & 0 \leq \psi \leq \zeta \\ 0, & \psi > \zeta \end{cases}, \quad (1)$$

where A_{pd} is the physical area of the receiver photo-detector, Z_v represents the Euclidean distance between the user and the nearest OBS, ϕ is the radiance angle of the nearest OBS with respect to the user, ψ is the angle of incidence from the nearest OBS to the user, ζ is the receiver FOV, and m is the Lambertian emission order given by $m = \ln(2)/\ln(\cos(\Theta_{1/2}))$. The half-power semi-angle ($\Theta_{1/2}$) denotes the angle of radiance at which the transmitted optical power gets half when compared to the power at $\phi = 0$. $T(\zeta)$ is the gain of the optical filter at the receiver and $G(\zeta) = n^2/\sin^2(\zeta)$ is the gain of the non-imaging concentrator where n is the refractive index. As mentioned earlier, it is assumed that the user moves along the horizontal axis with the photo-detector facing upward, which implies that $\phi = \psi$. Given the fact that $\cos(\phi) = \cos(\psi) = \frac{h_v}{Z_v}$, G can be simplified to

$$G = \begin{cases} \frac{A_{\text{pd}}(m+1)G(\zeta)T(\zeta)h_v^{m+1}}{2\pi Z_v^{m+3}}, & 0 \leq \psi \leq \zeta \\ 0, & \psi > \zeta \end{cases}. \quad (2)$$

In the next section, we will discuss the mathematical framework to characterize the mean and the distribution of sojourn time.

III. MATHEMATICAL FRAMEWORK

In this section, we present the mathematical model for the characterization of sojourn time and discuss the key steps involved in the mathematical modeling. The key steps involved in the mathematical analysis are as follows: 1) Obtaining association probabilities and service distance distributions for each tier. 2) Calculating the conditional distribution of sojourn time in the cell where the connection is initiated. 3) Obtaining the linear contact distribution function given that the test user is connected to a k^{th} tier BS at time 0. 4) Deriving the chord length distribution. 5) Calculating the mean and the distribution of sojourn time. A similar approach was considered in [36] to characterize the mean and the distribution of sojourn

time in multi-tier RF networks. However, [36] did not include the BSs' heights into the mathematical analysis. As per [58], incorporating BSs' heights into the analysis is necessary due to its impact on the network performance, however, the resulting mathematical model is not straightforward.

A. Association and Distance Analysis

As stated earlier, the sojourn time accounts for the time duration spent within the coverage area of a cell before changing the user-to-BS association. Thus, the mean and the distribution of sojourn time directly depend on the user-to-BS association probabilities. Under the RSS association policy, the user associates to the VLC if it offers the best received signal strength and thus the VLC association probability can be written as

$$A_{\text{VLC}} = \mathbb{P}[P^{\text{VLC}} > P^{\text{RF}}] = \mathbb{P}[P^{\text{VLC}} > P^{\text{RF}}, \psi \leq \zeta] + \mathbb{P}[P^{\text{VLC}} > P^{\text{RF}}, \psi > \zeta]. \quad (3)$$

Further mathematical manipulation and using the fact that $G = 0$ for $\psi > \zeta$ lead to

$$A_{\text{VLC}} = \mathbb{E}_{Z_r} \left\{ \mathbb{P}[Z_r > D_{\text{vr}} Z_v^{\alpha_{\text{vr}}}, \psi \leq \zeta] \right\}, \quad (4)$$

where

$$D_{\text{vr}} = \left(\frac{4\pi^2 K B_r P_r h_v^{-2(m+1)}}{B_v P_{\text{elec}} R_{\text{pd}}^2 (m+1)^2 A_{\text{pd}}^2 G^2(\zeta) T^2(\zeta)} \right)^{\frac{1}{\eta}}, \quad (5)$$

$$\alpha_{\text{vr}} = \frac{2(m+3)}{\eta}, \quad (6)$$

and B_k represents the k^{th} tier bias factor. Similarly, the RF association probability can be obtained as

$$A_{\text{RF}} = \mathbb{E}_{Z_r} \left\{ \mathbb{P}[Z_v > D_{\text{rv}} Z_r^{\alpha_{\text{rv}}}, \psi \leq \zeta] \right\} + \mathbb{P}[\psi > \zeta], \quad (7)$$

where $D_{\text{rv}} = \left(\frac{1}{D_{\text{vr}}}\right)^{\alpha_{\text{rv}}}$ and $\alpha_{\text{rv}} = \frac{1}{\alpha_{\text{vr}}}$. Finally, the VLC and the RF association probabilities in a PPP based two tier network are given by [44] where

$$Q = \begin{cases} \min \left[D_{\text{rv}} h_r^{\alpha_{\text{rv}}}, h_v \sqrt{1 + \tan^2(\zeta)} \right], & h_v \leq D_{\text{rv}} h_r^{\alpha_{\text{rv}}} \\ h_v, & \text{otherwise} \end{cases}, \quad (10)$$

$$P_0 = 1 - e^{-\pi \lambda_v h_v^2 \tan^2(\zeta)}, \quad (11)$$

and

$$\vartheta_k(u, w, Z_k, \chi) = \int_u^w \chi f_{Z_k}(z) dz. \quad (12)$$

Furthermore, $f_{Z_k}(z)$ is the probability density function (PDF) of the Euclidean distance between the user and the nearest k^{th} tier BS and is given by

$$f_{Z_r}(z) = 2\pi \lambda_r z e^{-\pi \lambda_r (z^2 - h_r^2)}, \quad h_r < z < \infty, \quad (13)$$

$$f_{Z_v}(z) = 2\pi \lambda_v z e^{-\pi \lambda_v (z^2 - h_v^2)}, \quad h_v < z < h_v \sqrt{1 + \tan^2(\zeta)}. \quad (14)$$

$$A_{\text{VLC}} = \underbrace{1 - e^{-\pi\lambda_v(Q-h_v)(Q+h_v)}}_{\triangleq A_{\text{VLC}_1}} + \underbrace{\vartheta_v \left(Q, h_v \sqrt{1 + \tan^2(\zeta)}, Z_v, e^{-\pi\lambda_r(D_{\text{vr}}^2 x^{2\alpha_{\text{vr}}} - h_r^2)} \right)}_{\triangleq A_{\text{VLC}_2}}, \quad (8)$$

$$A_{\text{RF}} = \begin{cases} \underbrace{\left(1 - P_0 + P_0 \left(1 - e^{-\pi\lambda_r(D_{\text{vr}}h_v^{\alpha_{\text{vr}}} - h_r)(D_{\text{vr}}h_v^{\alpha_{\text{vr}}} + h_r)} \right) \right)}_{\triangleq A_{\text{RF}_1}} + \underbrace{\left(D_{\text{vr}}h_v^{\alpha_{\text{vr}}} \right)}_{\triangleq A_{\text{RF}_2}} & h_r \leq D_{\text{vr}}h_v^{\alpha_{\text{vr}}} \\ \underbrace{\vartheta_r \left(D_{\text{vr}}h_v^{\alpha_{\text{vr}}}, \frac{D_{\text{vr}}h_v^{\alpha_{\text{vr}}}}{(1 + \tan^2(\zeta))^{-\frac{\alpha_{\text{vr}}}{2}}}, Z_r, P_0 - 1 + e^{-\pi\lambda_v(D_{\text{rv}}^2 x^{2\alpha_{\text{rv}}} - h_v^2)} \right)}_{\triangleq A_{\text{RF}_3}} & \\ 1 - P_0, & h_r \geq \frac{D_{\text{vr}}h_v^{\alpha_{\text{vr}}}}{(1 + \tan^2(\zeta))^{-\frac{\alpha_{\text{vr}}}{2}}} \\ 1 - P_0 + \vartheta_r \left(h_r, \frac{D_{\text{vr}}h_v^{\alpha_{\text{vr}}}}{(1 + \tan^2(\zeta))^{-\frac{\alpha_{\text{vr}}}{2}}}, Z_r, P_0 - 1 + e^{-\pi\lambda_v(D_{\text{rv}}^2 x^{2\alpha_{\text{rv}}} - h_v^2)} \right), & \text{Otherwise} \end{cases} \quad (9)$$

In stochastic geometry based analysis, the performance metrics are averaged over all possible user locations to obtain the spatial averages. This requires the characterization of service distance distributions of the RBSs and the OBSs. Let X_k , $k \in \{r, v\}$ be the horizontal distances between the user and the projection of the serving BS on the ground provided that the association is with the k^{th} tier BS. Then, the service distance distributions for the RBS and the OBS are given in (15) and (16), respectively [44].

$$f_{X_r}(x) = \begin{cases} \frac{2\pi\lambda_r x e^{-\pi\lambda_r x^2}}{A_{\text{RF}_1}(1 - e^{-\pi\lambda_r L_{r1}^2}) + A_{\text{RF}_2}}, & 0 \leq x \leq L_{r1} \\ \frac{2\pi\lambda_r x e^{-\pi\lambda_r x^2 - \pi\lambda_v((x^2 + h_r^2)^{\alpha_{\text{rv}}} D_{\text{rv}}^2 - h_v^2)}}{A_{\text{RF}_1}(e^{-\pi\lambda_r L_{r1}^2} - e^{-\pi\lambda_r L_{r2}^2}) + A_{\text{RF}_3}}, & L_{r1} < x \leq L_{r2} \\ \frac{(1 - P_0)2\pi\lambda_r x e^{-\pi\lambda_r x^2}}{A_{\text{RF}_1} e^{-\pi\lambda_r L_{r2}^2}}, & L_{r2} < x \leq \infty \end{cases} \quad (15)$$

$$f_{X_v}(x) = \begin{cases} \frac{2\pi}{A_{\text{VLC}_1}} \lambda_v x e^{-\pi\lambda_v x^2}, & 0 \leq x \leq L_v \\ \frac{2\pi}{A_{\text{VLC}_2}} \lambda_v x e^{-\pi\lambda_v x^2} e^{-\pi\lambda_r(D_{\text{vr}}^2(x^2 + h_v^2)^{\alpha_{\text{vr}}} - h_r^2)}, & L_v \leq x \leq h_v \tan(\zeta) \end{cases} \quad (16)$$

where A_{VLC_i} and A_{RF_i} represent the VLC and RF association probabilities given in (8) and (9), respectively, and

$$L_{r1} = \begin{cases} \sqrt{D_{\text{vr}}^2 h_v^{2\alpha_{\text{vr}}} - h_r^2}, & h_r \leq D_{\text{vr}}h_v^{\alpha_{\text{vr}}} \\ 0, & \text{otherwise} \end{cases},$$

$$L_{r2} = \begin{cases} \sqrt{\frac{D_{\text{vr}}^2 h_v^{2\alpha_{\text{vr}}}}{(1 + \tan^2(\zeta))^{-\frac{\alpha_{\text{vr}}}{2}}} - h_r^2}, & h_r \leq \frac{D_{\text{vr}}h_v^{\alpha_{\text{vr}}}}{(1 + \tan^2(\zeta))^{-\frac{\alpha_{\text{vr}}}{2}}} \\ 0, & \text{otherwise} \end{cases},$$

$$L_v = \sqrt{Q^2 - h_v^2}.$$

B. Conditional Distribution of Sojourn Time

In this section, we calculate the conditional distribution of sojourn time \hat{S}_k in a k^{th} tier cell where the connection was initiated. Let $\text{BS}(t)$ represent the serving BS at time t , then the conditional distribution of sojourn time in the cell where the connection is initiated can be calculated as

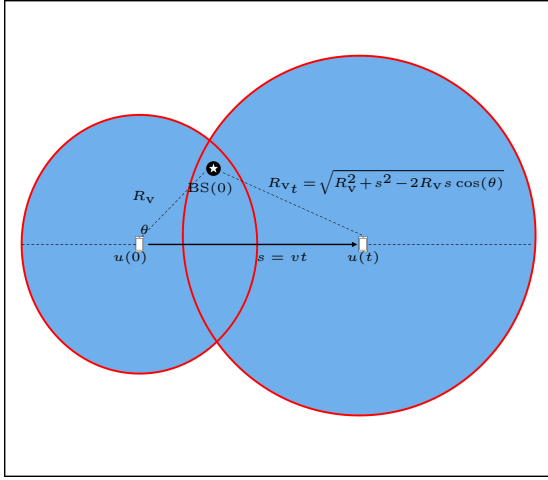
$$F_{\hat{S}_k}(T|\text{tier} = k) = 1 - \mathbb{P}(\text{BS}(0) = \text{BS}(t), \forall t \in (0, T]|\text{tier} = k) \quad (17)$$

Here, $\text{BS}(0) = \text{BS}(t)$ implies that the serving BS at time 0 and t is same. Since the coverage areas in the multi-tier networks may not be convex, there could be a situation between time 0 and T where $\text{BS}(0) \neq \text{BS}(t)$. Such a situation is referred to as a ping-pong HO where the user performs a HO back to the previous cell after spending some time in the new cell. This has been catered in (17) as we consider $\text{BS}(0) = \text{BS}(t), \forall t \in (0, T]$. By averaging over the user location, the conditional sojourn time distribution can be written as

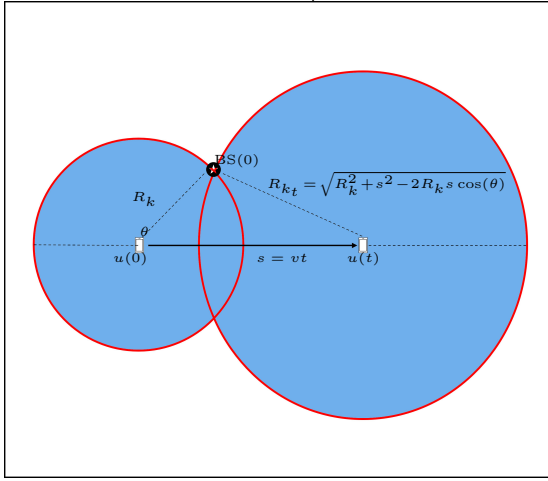
$$F_{\hat{S}}(T|\text{tier} = k) = 1 - \frac{1}{\pi} \int_0^\infty \int_0^\pi \mathbb{P}(\text{BS}(0) = \text{BS}(t), \forall t \in (0, T] | x, \theta, \text{tier} = k) f_{X_k}(x) d\theta dx \quad (18)$$

where $\theta \sim U[0, \pi]$ represents the angle between the serving BS at time 0 and the direction of movement of the user and $f_{X_k}(x)$ is given in (15) for RF and in (16) for VLC.

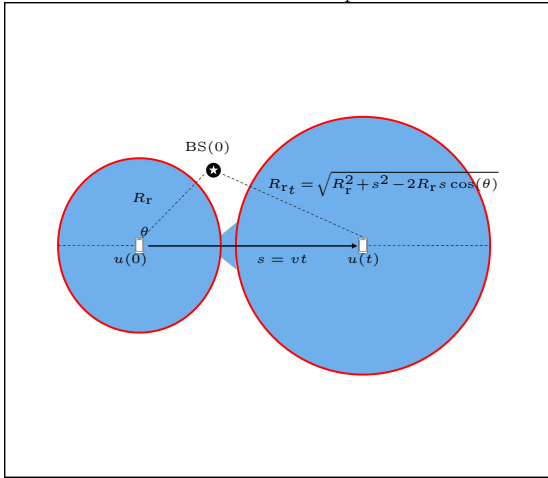
Let $u(t)$ denote the mobile user location at time t and R_{k_t} represent the horizontal distance between the mobile user and the nearest k^{th} tier BS at time t . For notational convenience, let R_k represent the horizontal distance between the mobile user and the nearest k^{th} tier BS at time 0. Given that at time t , the mobile user is connected to the k^{th} tier BS, we have $\Phi_j(\mathcal{B}(u(T), \sqrt{D_{kj}^2(R_{k_t}^2 + h_k^2)^{\alpha_{kj}}} - h_j^2))) = 0, \forall j \in \mathcal{K}$, where $\mathcal{B}(c, d)$ represents a ball centered at c with radius d and $\Phi_j(A)$ represents the number of j^{th} tier BSs in set $A \subset \mathbb{R}^2$.



(a) $\mathcal{A}_{vr}(R_v, v, T, \frac{\pi}{4}, 1.06, 2.17)$



(b) $\mathcal{A}_{kk}(R_k, v, T, \frac{\pi}{4}, 1, 1)$



(c) $\mathcal{A}_{rv}(R_r, v, T, \frac{\pi}{4}, 0.97, 0.46)$

Fig. 3: $\mathcal{A}_{kj}(R_k, v, T, \theta, D_{kj}, \alpha_{kj})$ for different network parameters. The black star represents the serving BS at time 0. The red circles represent $\mathcal{B}(u(0), \sqrt{D_{kj}^2(R_{k_0}^2 + h_k^2)^{\alpha_{kj}} - h_j^2})$ and $\mathcal{B}(u(T), \sqrt{D_{kj}^2(R_{k_t}^2 + h_k^2)^{\alpha_{kj}} - h_j^2})$.

Now the probability that no HO occurs between time 0 and t

such that the user is connected to the k^{th} tier BS is given by

$$\begin{aligned} \mathbb{P}(\text{BS}(0) = \text{BS}(t), \forall t \in (0, T] | x, \theta, \text{tier} = k) \\ = \mathbb{P}\left(\bigcap_{j \in \mathcal{K}} \left\{ \Phi_j\left(\mathcal{B}\left(u(T), \sqrt{D_{kj}^2(R_{k_t}^2 + h_k^2)^{\alpha_{kj}} - h_j^2}\right) \setminus \mathcal{B}\left(u(0), \sqrt{D_{kj}^2(R_k^2 + h_k^2)^{\alpha_{kj}} - h_j^2}\right)\right) = 0 \right\}, \forall t \in (0, T] | x, \theta, \text{tier} = k\right), \end{aligned} \quad (19)$$

where $D_{kk} = D_{jj} = 1$ and $\alpha_{kk} = \alpha_{jj} = 1$. Note that $\mathcal{B}\left(u(0), \sqrt{D_{kj}^2(R_k^2 + h_k^2)^{\alpha_{kj}} - h_j^2}\right)$ is excluded as no BS other than the serving BS is closer than $\sqrt{D_{kj}^2(R_k^2 + h_k^2)^{\alpha_{kj}} - h_j^2}$ to the test user at time 0. Let $s = vt$ represent the distance between $u(0)$ and $u(t)$. Then, using the law of cosines, R_{k_t} can be obtained as

$$R_{k_t} = \sqrt{R_k^2 + s^2 - 2R_k s \cos(\theta)}. \quad (20)$$

Now, the conditional probability in (19) can be written as

$$\begin{aligned} \mathbb{P}(\text{BS}(0) = \text{BS}(t), \forall t \in (0, T] | x, \theta, \text{tier} = k) = \\ \mathbb{P}\left(\bigcap_{j \in \mathcal{K}} \left\{ \Phi_j\left(\mathcal{A}_{kj}(R_k, v, T, \theta, D_{kj}, \alpha_{kj}) \setminus \mathcal{B}\left(u(0), \sqrt{D_{kj}^2(R_k^2 + h_k^2)^{\alpha_{kj}} - h_j^2}\right)\right) = 0 \right\}, | R_k, \theta, \text{tier} = k\right), \end{aligned} \quad (21)$$

where

$$\begin{aligned} \mathcal{A}_{kj}(R_k, v, T, \theta, D_{kj}, \alpha_{kj}) = \\ \left\{ \bigcup_t \mathcal{B}\left(u(T), \sqrt{D_{kj}^2(R_{k_t}^2 + h_k^2)^{\alpha_{kj}} - h_j^2}\right) | t \in (0, T], R_{k_t} \right\}. \end{aligned} \quad (22)$$

Using the fact that the two PPPs are independent, the conditional probability in (21) can be simplified to

$$\begin{aligned} \mathbb{P}(\text{BS}(0) = \text{BS}(t), \forall t \in (0, T] | x, \theta, \text{tier} = k) \\ = \prod_{j \in \mathcal{K}} \mathbb{P}\left(\Phi_j\left(\mathcal{A}_{kj}(R_k, v, T, \theta, D_{kj}, \alpha_{kj}) \setminus \mathcal{B}\left(u(0), \sqrt{D_{kj}^2(R_k^2 + h_k^2)^{\alpha_{kj}} - h_j^2}\right)\right) = 0, | R_k, \theta, \text{tier} = k\right), \\ \stackrel{(a)}{=} \prod_{j \in \mathcal{K}} \exp\left(-\lambda_j \left| \mathcal{A}_{kj}(R_k, v, T, \theta, D_{kj}, \alpha_{kj}) \setminus \mathcal{B}\left(u(0), \sqrt{D_{kj}^2(R_k^2 + h_k^2)^{\alpha_{kj}} - h_j^2}\right) \right|\right), \end{aligned} \quad (23)$$

where (a) results from the void probability of PPP, and $|\mathcal{A}_{kj}|$ represents the area of \mathcal{A}_{kj} . Depending upon the network parameters, \mathcal{A}_{kj} corresponds to three different scenarios as il-

lustrated in Fig. 3. Since $\mathcal{B}\left(u(0), \sqrt{D_{kj}^2(R_k^2 + h_k^2)^{\alpha_{kj}} - h_j^2}\right) \subset \mathcal{A}_{kj}(R_k, v, T, \theta, D_{kj}, \alpha_{kj})$, (21) can be written as

$$\mathbb{P}(\text{BS}(0) = \text{BS}(t), \forall t \in (0, T] | x, \theta, \text{tier} = k) = \exp\left(\sum_{j \in \mathcal{K}} -\lambda_j \left(\left|\mathcal{A}_{kj}(R_k, v, T, \theta, D_{kj}, \alpha_{kj})\right| - \pi(D_{kj}^2(R_k^2 + h_k^2)^{\alpha_{kj}} - h_j^2)\right)\right). \quad (24)$$

In order to compute the mean and the distribution of sojourn time, the calculation of $|\mathcal{A}_{kj}(\cdot, \cdot, \cdot, \cdot, \cdot)|$ is required, which is discussed in the following sections.

1) *Computation of \mathcal{A}_{vr}* : Due to the disparity in the powers and the channel gains of RF and VLC technologies, \mathcal{A}_{vr} can be visualized as an overlap of $\mathcal{B}\left(u(0), \sqrt{D_{vr}^2(R_v^2 + h_v^2)^{\alpha_{vr}} - h_r^2}\right)$ and $\mathcal{B}\left(u(T), \sqrt{D_{vr}^2(R_v^2 + h_v^2)^{\alpha_{vr}} - h_r^2}\right)$. This is illustrated in Fig. 3(a). The computation of \mathcal{A}_{vr} depends on the radii of the two circles and the distance between their centres. Thus, the following cases can occur.

Case 1:

When we have the radius of one circle greater than that of the other by s i.e.,

$$\sqrt{D_{vr}^2(R_v^2 + h_v^2)^{\alpha_{vr}} - h_r^2} \geq \sqrt{D_{vr}^2(R_v^2 + h_v^2)^{\alpha_{vr}} - h_r^2} + s, \text{ then,}$$

$$\mathcal{B}\left(u(0), \sqrt{D_{vr}^2(R_v^2 + h_v^2)^{\alpha_{vr}} - h_r^2}\right) \subset \mathcal{B}\left(u(T), \sqrt{D_{vr}^2(R_v^2 + h_v^2)^{\alpha_{vr}} - h_r^2}\right),$$

which results in

$$\mathcal{A}_{vr}(R_v, v, T, \theta, D_{vr}, \alpha_{vr}) = \mathcal{B}\left(u(T), \sqrt{D_{vr}^2(R_v^2 + h_v^2)^{\alpha_{vr}} - h_r^2}\right).$$

Case 2:

Similarly, when $\sqrt{D_{vr}^2(R_v^2 + h_v^2)^{\alpha_{vr}} - h_r^2} \geq \sqrt{D_{vr}^2(R_v^2 + h_v^2)^{\alpha_{vr}} - h_r^2} + s$, then,

$$\mathcal{B}\left(u(T), \sqrt{D_{vr}^2(R_v^2 + h_v^2)^{\alpha_{vr}} - h_r^2}\right) \subset \mathcal{B}\left(u(0), \sqrt{D_{vr}^2(R_v^2 + h_v^2)^{\alpha_{vr}} - h_r^2}\right),$$

and hence results in

$$\mathcal{A}_{vr}(R_v, v, T, \theta, D_{vr}, \alpha_{vr}) = \mathcal{B}\left(u(0), \sqrt{D_{vr}^2(R_v^2 + h_v^2)^{\alpha_{vr}} - h_r^2}\right).$$

Case 3:

When $\sqrt{D_{vr}^2(R_v^2 + h_v^2)^{\alpha_{vr}} - h_r^2} < \sqrt{D_{vr}^2(R_v^2 + h_v^2)^{\alpha_{vr}} - h_r^2} + s$, and $\sqrt{D_{vr}^2(R_v^2 + h_v^2)^{\alpha_{vr}} - h_r^2} < \sqrt{D_{vr}^2(R_v^2 + h_v^2)^{\alpha_{vr}} - h_r^2} + s$, then,

$$\mathcal{A}_{vr}(R_v, v, T, \theta, D_{vr}, \alpha_{vr}) = \mathcal{B}\left(u(0), \sqrt{D_{vr}^2(R_v^2 + h_v^2)^{\alpha_{vr}} - h_r^2}\right) \cup \mathcal{B}\left(u(T), \sqrt{D_{vr}^2(R_v^2 + h_v^2)^{\alpha_{vr}} - h_r^2}\right).$$

As we have highlighted the regions of interest, we can now compute $|\mathcal{A}_{vr}(R_v, v, T, \theta, D_{vr}, \alpha_{vr})|$, which is given in the following lemma.

Lemma 1: The area of the region where the user maintains its connection to the nearest OBS while it covers the distance

s in time t along the direction θ with respect to the projection of OBS on the ground is given in (25).

Proof: See Appendix A.

2) *Computation of \mathcal{A}_{kk}* : Next, we compute the area of $\mathcal{A}_{kk}(R_k, v, T, \theta, 1, 1)$, which can be visualized via Fig. 3(b). Note that this case corresponds to a single tier scenario where no k^{th} tier BS is closer than the serving BS as the user moves from $u(0)$ to $u(T)$. Thus, the region of interest will be $\mathcal{B}(u(0), R_k) \cup \mathcal{B}(u(T), R_k)$. The resulting area is given in the following lemma.

Lemma 2: The area of the region where no k^{th} tier BS is closer than the serving BS as the user travels the distance s from $u(0)$ to $u(T)$ is given by

$$\begin{aligned} \mathcal{A}_{kk}(R_k, v, T, \theta, 1, 1) &= R_k^2[\pi - \arccos(\cos(\theta))] + R_k s \\ &\times \sqrt{1 - \cos^2(\theta)} + [R_k^2 + s^2 - 2R_k s \cos(\theta)] \\ &\times \arccos\left(\frac{R_k \cos(\theta) - s}{\sqrt{R_k^2 + s^2 - 2R_k s \cos(\theta)}}\right) \end{aligned} \quad (26)$$

Proof: See Appendix B.

3) *Computation of \mathcal{A}_{rv}* : Now, we compute the area of $\mathcal{A}_{rv}(R_r, v, T, \theta, D_{rv}, \alpha_{rv})$, which can be visualized via Fig. 3(c). In this case, we study the intersection between $\mathcal{B}\left(u(t), \sqrt{D_{rv}^2(R_r^2 + h_r^2)^{\alpha_{rv}} - h_v^2}\right)$ and $\mathcal{B}\left(u(t + dt), \sqrt{D_{rv}^2(R_r^2 + h_r^2)^{\alpha_{rv}} - h_v^2}\right)$ as $dt \rightarrow 0$, where $R_{r,t+dt}^2$ is obtained from the triangle equations and is given by

$$R_{r,t+dt}^2 = R_{rt}^2 + v^2 dt^2 + 2vdt(vt - R_r \cos(\theta)). \quad (27)$$

As $dt \rightarrow 0$, $\mathcal{B}\left(u(t), \sqrt{D_{rv}^2(R_r^2 + h_r^2)^{\alpha_{rv}} - h_v^2}\right)$ and $\mathcal{B}\left(u(t + dt), \sqrt{D_{rv}^2(R_r^2 + h_r^2)^{\alpha_{rv}} - h_v^2}\right)$ partially overlap and results in (28). Finally, the area of $\mathcal{A}_{rv}(R_r, v, T, \theta, D_{rv}, \alpha_{rv})$ is given in the following lemma.

Lemma 3: The area of the region where the user having an initial connection with the RBS retains its connection as it moves from $u(0)$ to $u(t)$ is given in (29).

Proof: See Appendix C.

Now that we have calculated the areas of the desired regions, we will plug these areas into (24) and substitute the result in (18) and obtain the conditional sojourn time distribution. In the next section, we compute the linear contact and chord length distributions to calculate the tier- k sojourn time distribution and the mean sojourn time.

C. Linear Contact and Chord Length Distributions

The linear contact distribution is defined as the probability that a line containing the origin passes through the cell boundaries. In particular, given the origin lying inside a tier- k cell boundary, the linear contact distribution function is equal to the probability that the intersection between the user trajectory of length s and the cell boundaries is non-empty.

$$\begin{aligned}
 & |\mathcal{A}_{vT}(R_v, v, T, \theta, D_{vT}, \alpha_{vT})| = \\
 & \begin{cases} \pi \left(D_{vT}^2 (R_v^2 + h_v^2)^{\alpha_{vT}} + \frac{\alpha_{vT} D_{vT}^2 (s^2 - 2R_v s \cos(\theta))}{(R_v^2 + h_v^2)^{1-\alpha_{vT}}} - h_r^2 \right), & \theta \geq \arccos \left(\frac{s(\alpha_{vT} D_{vT}^2 (R_v^2 + h_v^2)^{\alpha_{vT}-1} - 1) - 2\sqrt{D_{vT}^2 (R_v^2 + h_v^2)^{\alpha_{vT}} - h_r^2}}{2\alpha_{vT} D_{vT}^2 R_v (R_v^2 + h_v^2)^{\alpha_{vT}-1}} \right) \\ \pi \left(D_{vT}^2 (R_v^2 + h_v^2)^{\alpha_{vT}} - h_r^2 \right), & \theta \leq \arccos \left(\frac{s(\alpha_{vT} D_{vT}^2 (R_v^2 + h_v^2)^{\alpha_{vT}-1} - 1) + 2\sqrt{D_{vT}^2 (R_v^2 + h_v^2)^{\alpha_{vT}} - h_r^2}}{2\alpha_{vT} D_{vT}^2 R_v (R_v^2 + h_v^2)^{\alpha_{vT}-1}} \right) \\ (D_{vT}^2 (R_v^2 + h_v^2)^{\alpha_{vT}} - h_r^2) \arccos \left(\frac{s(\alpha_{vT} D_{vT}^2 (R_v^2 + h_v^2)^{\alpha_{vT}-1} - 1) - 2\alpha_{vT} D_{vT}^2 R_v (R_v^2 + h_v^2)^{\alpha_{vT}-1} \cos(\theta)}{2\sqrt{D_{vT}^2 (R_v^2 + h_v^2)^{\alpha_{vT}} - h_r^2}} \right), & \text{Otherwise} \end{cases} \\
 & + (D_{vT}^2 (R_v^2 + h_v^2)^{\alpha_{vT}} - h_r^2 + \alpha_{vT} D_{vT}^2 (R_v^2 + h_v^2)^{\alpha_{vT}-1} (s^2 - 2R_v s \cos(\theta))) \\
 & \times \arccos \left(\frac{2\alpha_{vT} D_{vT}^2 R_v (R_v^2 + h_v^2)^{\alpha_{vT}-1} \cos(\theta) - s(1 + \alpha_{vT} D_{vT}^2 (R_v^2 + h_v^2)^{\alpha_{vT}-1})}{2\sqrt{D_{vT}^2 (R_v^2 + h_v^2)^{\alpha_{vT}} + \alpha_{vT} D_{vT}^2 (R_v^2 + h_v^2)^{\alpha_{vT}-1} (s^2 - 2R_v s \cos(\theta)) - h_r^2}} \right) \\
 & + \frac{1}{2} \sqrt{4s^2 (D_{vT}^2 (R_v^2 + h_v^2)^{\alpha_{vT}} - h_r^2) - (s^2 - \alpha_{vT}^2 D_{vT}^2 (R_v^2 + h_v^2)^{\alpha_{vT}-1} (s^2 - 2R_v s \cos(\theta)))^2}
 \end{aligned} \tag{25}$$

$$\begin{aligned}
 & \left| \mathcal{B}(u(t), \sqrt{D_{rv}^2 (R_t^2 + h_r^2)^{\alpha_{rv}} - h_v^2}) \setminus \mathcal{B}(u(t+dt), \sqrt{D_{rv}^2 (R_{t+dt}^2 + h_r^2)^{\alpha_{rv}} - h_v^2}) \right| \\
 & = 2v \left[\sqrt{D_{rv}^2 (R_t^2 + h_r^2)^{\alpha_{rv}} - h_v^2} - [\alpha_{rv} D_{rv}^2 (R_t^2 + h_r^2)^{\alpha_{rv}-1} (vt - R_r \cos(\theta))] \right]^2 \\
 & \quad - \alpha_{rv} D_{rv}^2 (R_t^2 + h_r^2)^{\alpha_{rv}-1} (vt - R_r \cos(\theta)) \arccos \left(\frac{\alpha_{rv} D_{rv}^2 (R_t^2 + h_r^2)^{\alpha_{rv}-1} (vt - R_r \cos(\theta))}{\sqrt{D_{rv}^2 (R_t^2 + h_r^2)^{\alpha_{rv}} - h_v^2}} \right) \Big] dt \tag{28}
 \end{aligned}$$

$$\begin{aligned}
 & |\mathcal{A}_{rv}(R_r, v, T, \theta, D_{rv}, \alpha_{rv})| = \pi [D_{rv}^2 (R_r^2 + s^2 - 2R_r s \cos(\theta) + h_r^2)^{\alpha_{rv}} - h_v^2] \\
 & \quad + 2s \int_0^1 \sqrt{D_{rv}^2 (R_r^2 + s^2 - 2R_r s \cos(\theta) + h_r^2)^{\alpha_{rv}} - h_v^2} - \left[\frac{\alpha_{rv} D_{rv}^2 (su - R_r \cos(\theta))}{(R_r^2 + s^2 - 2R_r s \cos(\theta) + h_r^2)^{1-\alpha_{rv}}} \right]^2 \\
 & \quad - \frac{\alpha_{rv} D_{rv}^2 (su - R_r \cos(\theta))}{(R_r^2 + s^2 - 2R_r s \cos(\theta) + h_r^2)^{1-\alpha_{rv}}} \arccos \left(\frac{\alpha_{rv} D_{rv}^2 (R_r^2 + s^2 - 2R_r s \cos(\theta) + h_r^2)^{\alpha_{rv}-1} (su - R_r \cos(\theta))}{\sqrt{D_{rv}^2 (R_r^2 + s^2 - 2R_r s \cos(\theta) + h_r^2)^{\alpha_{rv}} - h_v^2}} \right) du \tag{29}
 \end{aligned}$$

Mathematically, it is related to the cumulative distribution function (CDF) of \hat{S} and thus can be written as

$$\mathcal{H}(s | \text{tier} = k) = \mathbb{P}(\hat{S}_k \leq \frac{s}{v} | \text{tier} = k) = F_{\hat{S}_k}(\frac{s}{v} | \text{tier} = k) \tag{30}$$

Until now, we have discussed the sojourn time in the cell where the connection was initiated, i.e., \hat{S} . Now we focus on the mean and the distribution of the sojourn time S_k for tier- k . The sojourn time distribution for tier- k is equivalent to the chord length distribution. Thus, the calculation of the chord length distribution function is required. The chord length distribution is related to the linear contact distribution by [50]

$$F_L(s | \text{tier} = k) = 1 - \mathbb{E}[L | \text{tier} = k] \frac{d}{ds} \mathcal{H}(s | \text{tier} = k), \tag{31}$$

where $\mathbb{E}[L | \text{tier} = k]$ represents the mean length of chords lying inside tier- k cells and is given by [59]

$$\mathbb{E}[L | \text{tier} = k] = \lim_{s \rightarrow 0} \frac{1}{\frac{d}{ds} \mathcal{H}(s | \text{tier} = k)}. \tag{32}$$

Now that we have the mean length of chords lying inside tier- k cells, the mean sojourn time can be obtained as shown in the following corollary.

Corollary 1: Given the mean length of chords lying inside k^{th} tier cells, the mean sojourn time in tier- k cells is given by

$$\mathbb{E}[S | \text{tier} = k] = \frac{1}{v} \mathbb{E}[L | \text{tier} = k] = \frac{1}{v} \lim_{s \rightarrow 0} \frac{1}{\frac{d}{ds} \mathcal{H}(s | \text{tier} = k)}, \tag{33}$$

where $\frac{d}{ds} \mathcal{H}(s | \text{tier} = k)|_{s=0}$ in (33) can be written as

$$\begin{aligned}
 & \frac{d}{ds} \mathcal{H}(s | \text{tier} = k)|_{s=0} = 1 - \frac{1}{\pi} \int_0^\infty \int_0^\pi \\
 & \left(\sum_{j \in \mathcal{K}} \lambda_j \frac{d}{ds} \left| \mathcal{A}_{kj}(R_k, v, T, \theta, D_{kj}, \alpha_{kj}) \right|_{s=0} \right) f_{X_k}(x) d\theta dx, \tag{34}
 \end{aligned}$$

and $\frac{d}{ds} \left| \mathcal{A}_{kj}(\cdot, \cdot, \cdot, \cdot, \cdot) \right|_{s=0}$ is given in (35) and (36). Finally, the distribution of the sojourn time for tier- k is given by the following theorem.

Theorem 1: The distribution of sojourn time in the k^{th} tier cells is given by

$$F_S(T | \text{tier} = k) = F_L(vT | \text{tier} = k), \tag{37}$$

$$\frac{d}{ds} \left| \mathcal{A}_{vr}(R_v, v, T, \theta, D_{vr}, \alpha_{vr}) \right|_{s=0} = \begin{cases} -2\pi\alpha_{vr}D_{vr}^2R_v(R_v^2 + h_v^2)^{\alpha_{vr}-1} \cos(\theta), & \theta \geq \pi - \arccos\left(\frac{\sqrt{D_{vr}(R_v^2 + h_v^2)^{\alpha_{vr}} - h_r^2}}{\alpha_{vr}D_{vr}^2R_v(R_v^2 + h_v^2)^{\alpha_{vr}-1}}\right) \\ 0, & \theta \leq \arccos\left(\frac{\sqrt{D_{vr}(R_v^2 + h_v^2)^{\alpha_{vr}} - h_r^2}}{\alpha_{vr}D_{vr}^2R_v(R_v^2 + h_v^2)^{\alpha_{vr}-1}}\right) \\ \sqrt{D_{vr}^2(R_v^2 + h_v^2)^{\alpha_{vr}} - h_r^2} - [\alpha_{vr}D_{vr}^2R_v(R_v^2 + h_v^2)^{\alpha_{vr}-1} \cos(\theta)]^2 \\ -2\alpha_{vr}D_{vr}^2R_v(R_v^2 + h_v^2)^{\alpha_{vr}-1} \cos(\theta) \arccos\left(\frac{\alpha_{vr}D_{vr}^2R_v(R_v^2 + h_v^2)^{\alpha_{vr}-1} \cos(\theta)}{\sqrt{D_{vr}^2(R_v^2 + h_v^2)^{\alpha_{vr}} - h_r^2}}\right), & \text{Otherwise} \end{cases} \quad (35)$$

$$\frac{d}{ds} \left| \mathcal{A}_{rv}(R_r, v, T, \theta, D_{rv}, \alpha_{rv}) \right|_{s=0} = 2\sqrt{D_{rv}^2(R_r^2 + h_r^2)^{\alpha_{rv}} - h_v^2} - [\alpha_{rv}D_{rv}^2(R_r^2 + h_r^2)^{\alpha_{rv}-1}R_r \cos(\theta)]^2 - 2\alpha_{rv}D_{rv}^2(R_r^2 + h_r^2)^{\alpha_{rv}-1}R_r \cos(\theta) \arccos\left(\frac{\alpha_{rv}D_{rv}^2(R_r^2 + h_r^2)^{\alpha_{rv}-1}R_r \cos(\theta)}{\sqrt{D_{rv}^2(R_r^2 + h_r^2)^{\alpha_{rv}} - h_v^2}}\right) \quad (36)$$

Proof: Given a user moving along a straight line with a fixed velocity, the probability that $S \leq T$ is equal to the probability that $L \leq vT$.

The computation of sojourn time distribution given in (37) requires the numerical evaluation of (18) and (34). Similar to [27] and [44], it is intractable to obtain closed form expressions in height aware models. Also, considering different channel models adds even more complexity to the mathematical model. Hence, numerical evaluation is required to obtain the results, which is however computationally less expensive than simulations². Note that the simulations require sufficient number of network realizations to account for the spatial randomness in the BSs' locations and long user trajectories such that the user passes through all user-to-BS association states. While the final mathematical expressions for the mean and the distribution of sojourn time are omitted due to brevity, the mathematical analysis evaluated at $h_r = h_v = 0$ and $\alpha_{rv} = \alpha_{vr} = 1$ results in similar sojourn time expressions (with disparity in BS powers) obtained in [36] for multi-tier RF networks. The mathematical model presented in this paper offers a road map to compute sojourn time in height aware heterogeneous networks with the disparity in the channel models. The sojourn time information can also help studying other important network KPIs e.g., HO failure probability and pin-pong HO rate. In what follows we discuss the numerical results and validate our mathematical model via Monte-Carlo simulations, which shows an average mean square error of 0.013 between analysis and simulations results.

IV. NUMERICAL RESULTS

We will now utilize the mathematical framework developed in this paper to analyze the impact of VLC centric parameters on the mean and the distribution of sojourn time. The developed mathematical model is necessary to investigate the relationship between different network parameters and helps

²Given a typical Intel core-i7 system @2.8GHz, the sojourn time distribution computation via numerical evaluation takes 2.5 seconds in comparison to 1075 seconds taken by the simulations involving parallel computing.

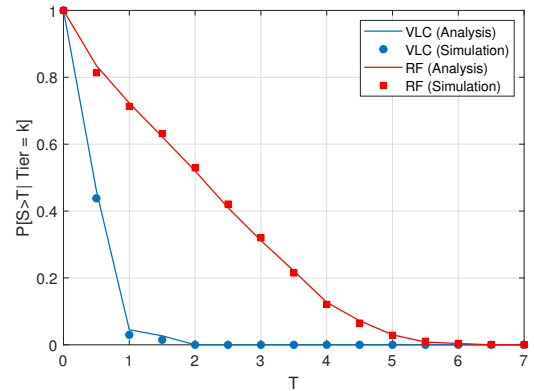


Fig. 4: Complementary CDFs of sojourn time in RBS and OBS coverage areas for $v = 3$ m/s.

highlighting the unnecessary HOs that can be avoided to enhance the network performance. In addition to the analytical PPP, we simulate other deployment models as shown in Fig. 1 and study the mean sojourn time for each deployment scenario. In the square lattice deployment, OBSs' locations are abstracted via a square lattice pattern while RBSs locations are modeled via a PPP. In MHCPP, the BSs' locations exhibit repulsion and thus are not allowed to be closer by a pre-defined distance. This deployment offers a more realistic modeling where the BSs do not coexist at the same location [60]. Further, we exploit the sojourn time distribution to highlight the unnecessary HO rate. The accuracy of PPP mathematical modeling is also validated via Monte-Carlo simulations. Fig. 4 shows the complementary CDFs of sojourn time in RF and VLC coverage areas where the RBSs and OBSs are modeled via PPPs. It is observed that the simulations results conform with the analytical results.

A. Simulation Setup

To bring fairness in the performance comparison of different deployment settings, the simulation area and the network parameters for all deployment cases are chosen in accordance

TABLE II: Simulation parameters in RF/VLC hybrid network [10]

| Parameter | Value |
|--|--------------------------|
| OBS Optical Power P_{opt} : | 40 dBm |
| RBS Power P_r : | 10 dBm |
| OBS Intensity λ_v : | 0.1648 BS/m ² |
| RBS Intensity λ_r : | 0.0087 BS/m ² |
| BSSs' heights h_r, h_v : | 2.5 m, 2.5 m |
| Refractive Index n : | 1.5 |
| Path loss exponent η : | 3.68 |
| Photo-detector Area A_{pd} : | 0.0001 m ² |
| Photo-detector Responsivity R_{pd} : | 0.6 A/W |
| Optical-to-electrical conversion ratio n_c : | 3 |
| Gain of Optical Filter $T(\zeta)$: | 1 |
| Half-power Semi-angle $\Theta_{1/2}$: | 60° |
| Carrier Frequency f_c : | 2.4 GHz |
| User velocity v : | 0.28 m/s |

with the actual scenario. A simulation area of 74 m x 31 m is considered, which represents the area of an academic block in the University of British Columbia, Canada. Moreover, the actual BSs intensities are used to generate the PPP and the square lattice deployments. For MHCPP, a PPP Φ_k is generated with intensity λ_k . Then, each point in the PPP is marked with a random number uniformly distributed on $[0, 1]$. A point is retained in the point process Φ_k if its mark is the largest among all the points located within a distance d_k and is removed otherwise. In order to bring fairness, the intensity of initial PPP Φ_k is considered higher than that of λ_k , i.e., $\lambda_k = -\ln(1 - \lambda_k \pi d_k^2) / \pi d_k^2$ [50].

For the validation of the analytical PPP modeling via simulations, we assume that the user moves in a straight line. The same assumption was considered in the mathematical analysis. Since the non-PPP models are less random (or more regular), a straight line mobility assumption will not be reasonable. Thus, in addition to the straight line mobility model for PPP validation, we also consider a simplified random way-point mobility model. In the simplified random way-point mobility model, the user moves a certain distance with the constant velocity along a random direction. In this paper, with a random orientation, the user moves a distance of 0.01 m in each step where there are 19916 steps per iteration. After each step, the direction of movement is randomly chosen from a uniform distribution, i.e., $U[0, 2\pi]$. To perform averaging, we consider 1000 iterations. During each iteration, the initial location of the user is chosen randomly. After each step taken by the user, the serving BS information is recorded, which is then used to calculate the sojourn time. A unity bias factor is considered unless stated otherwise. The simulation parameters are summarized in Table II where the RF parameters are the actual parameters of an indoor Wi-Fi network deployed in the university academic block and the VLC specific parameters are in accordance with [10]. Note that a similar simulation setup was considered in [44] to study HO rates in RF/VLC hybrid networks.

B. Mean Sojourn Time

First, we study the mean sojourn time in RF/VLC hybrid networks under different deployment models. Figs. 5(a) and 5(b) show the mean sojourn time for the VLC and the RF tiers, respectively. We observe that all the deployment models exhibit similar performance in terms of mean sojourn time, however, a closer match is observed with the increase in the user velocity. It is also noted that the simulation results obtained from both the straight line and the random way-point mobility models for PPP validate our analytical model. This is due to the fact that the homogeneous PPP is stationary and isotropic, i.e., its distribution is invariant under translation and rotation with respect to the origin [61]. Moreover, the similar performance of PPP and actual deployment scenario motivates the PPP assumption for sojourn time based studies. Next, we study the impact of BS density and receiver FOV on the mean sojourn time. Figs. 6(a) and 6(b) demonstrate the impact of the OBS density and receiver FOV on the VLC and RF tiers sojourn time, respectively. The following conclusions are drawn from Figs. 6(a) and 6(b). First, an increase in the OBS density reduces the mean sojourn time due to reduction in the coverage areas served by each BS. Second, an increase in the receiver FOV reduces the mean sojourn time in case of VLC but shows an increase in the case of RF. This is due to the fact that the increase in the receiver FOV pushes more traffic from the VLC to the RF by shrinking the VLC coverage footprints.

Due to the high density of OBSs, a mobile user may experience high OBS to OBS and RBS to OBS handovers, which may also include unnecessary HOs that impose signalling overhead and consume resources. Therefore, it is crucial to study unnecessary HOs that can be avoided to enhance the network performance. In the next section, we will exploit the sojourn time distribution to investigate the unnecessary HO probability in the RF/VLC hybrid network.

C. Unnecessary Handover Probability

A HO is considered unnecessary if the sojourn time in the new cell is less than a certain threshold. In practice, the unnecessary HOs are avoided by dragging the connection with the serving cell until the HO conditions are met, which may cause little degradation in the user rate. This can be realized by setting two HO conditions [35]. First, as soon as the user hits the cell boundary, a time to trigger (TTT) timer is started and the user performs the HO after the TTT timer is expired. This ensures that the received signal strength of the target BS is greater than that of the serving BS for at least TTT period. In 3GPP standards, such an event is referred to as A3 event where the RSS of the target BS is greater than that of the serving BS plus hysteresis margin [62]. Second, after associating to the new cell, the user should spend at least T_p time before handing over to another cell. Mathematically, we can write the unnecessary HO probability as [35], [36]

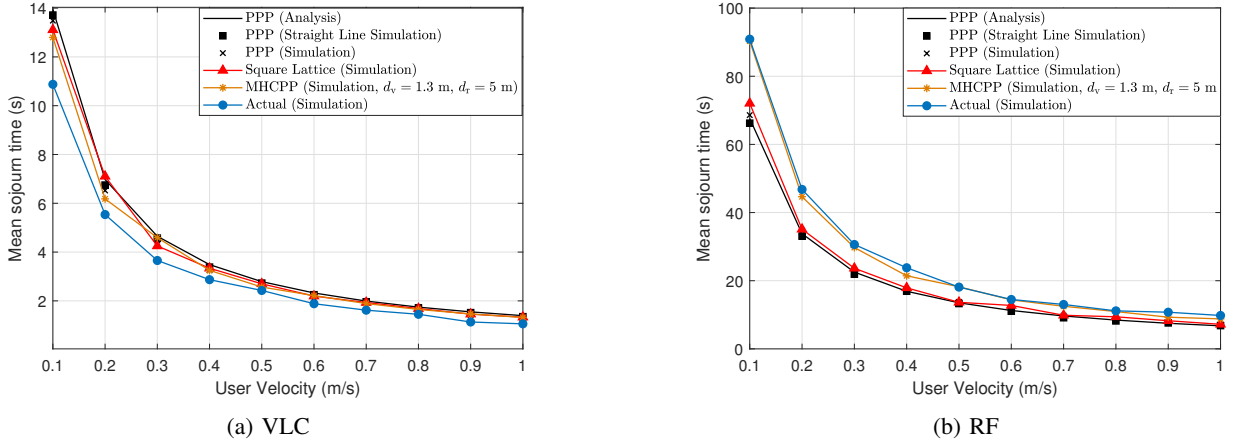


Fig. 5: Comparison of mean sojourn time under different BSs' deployment models.

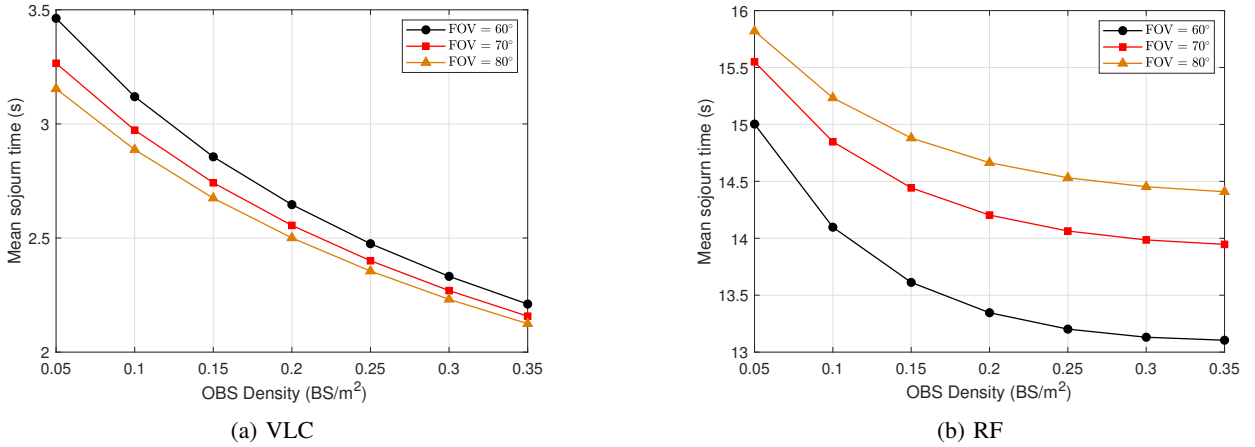


Fig. 6: Impact of receiver FOV on mean sojourn time.

$$\begin{aligned} \text{HO}_{\text{Unnecessary}} &= P[S < T_p | \text{tier} = k] - P[S < \text{TTT} | \text{tier} = k], \\ &= \bar{F}_S(\text{TTT} | \text{tier} = k) - \bar{F}_S(T_p | \text{tier} = k). \end{aligned} \quad (38)$$

First, we analyze the complementary sojourn time distribution $\bar{F}_S(T | \text{tier} = v)$ for different values of T versus user velocity as shown in Fig. 7. Considering $T_p = 0.5$ s and $\text{TTT} = 0.2$ s, which are the typical values used in the literature [36], the unnecessary HO probability can be obtained from the complementary distribution plot shown in Fig. 7. In addition to the unnecessary HO probability, the sojourn time distribution obtained in this paper can also be used to calculate the mean download time of a file [63]. Furthermore, a close match between simulations and analytical results validate our mathematical model.

Next, we investigate the impact of OBS density on the unnecessary HO probability. Fig. 8 shows the unnecessary HO probability versus user velocity for different OBS densities. The results indicate that the unnecessary HO probability reaches 0.38 as the user velocity reaches 3 m/s in a network with the actual BS density, i.e., $\lambda_v = 0.1648$ BS/m². Increasing density gives further rise to the unnecessary HO probability,

which calls for some efficient HO management techniques³. In general, the following conclusions can be drawn from the numerical results. The PPP, the MHCPP, and the square lattice models are all found to be good approximations for an actual hybrid RF/VLC network deployment as they capture the user mobility performance of the actual network. Hence, the PPP approximation for a hybrid RF/VLC network can be used for an analytical study of mobility aware performance metrics. Moreover, due to the high density of OBSs, a high unnecessary HO probability is observed, which requires the implementation of some HO skipping techniques to ensure provisioning of ubiquitous quality of service. Further, in contrast to the simulations, which are time consuming and computationally more expensive, the mathematical modeling presented in this paper can help researchers to reproduce results and utilize the mathematical framework to study sojourn time in future wireless networks having disparity in the channel models. Moreover, It

³A wide range of OBS densities has been considered in the literature to study the impact of BS density on the network performance. A recent survey on indoor user positioning shows that the OBS density ranging between 0.01 and 9.8 VLC transmitters/m² was considered in the experimental studies for estimating user location in indoor environments [64]. In highly dense networks, some handover skipping techniques are desired to minimize the impact of network density on the handover rates [18].

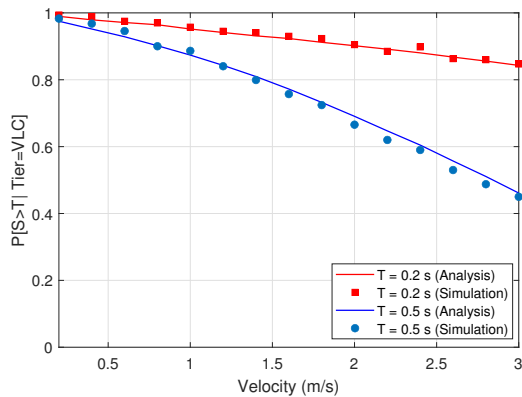


Fig. 7: Sojourn time distribution versus user velocity for different values of T .

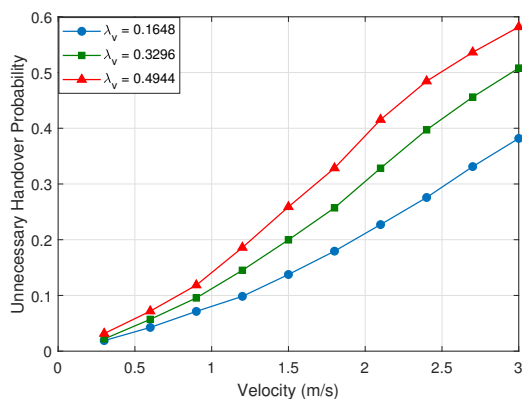


Fig. 8: Unnecessary HO probability for different OBS densities λ_v with $T_p = 0.5$ s and TTT = 0.2 s.

can also help analyzing sojourn time dependent performance metrics including HO rate, HO failure rate, channel holding time, and mean download time of a file in the RF/VLC hybrid networks.

V. CONCLUSION

This paper characterized the mean and the distribution of sojourn time in PPP based two-tier RF/VLC hybrid networks. Several BSs deployment scenarios including the MHCPP and the square lattice were considered and the mean sojourn time under each deployment case was compared to that of an actual deployment scenario. The numerical results show that the PPP, the MHCPP, and the square lattice deployments are good approximations for modeling the BSs' locations in RF/VLC hybrid networks. This supports the usefulness and applicability of PPP based mathematical modeling in RF/VLC hybrid network. Further, the impacts of user velocity, BS density, and the receiver FOV on the sojourn time were also studied. The results also highlighted unnecessary HO probability that reaches up to 0.38 with the actual density, which calls for some efficient HO management and skipping techniques.

APPENDIX

A. Proof of Lemma 1

For case 1, the area of \mathcal{A}_{vr} can be simply calculated via the formula of circle with radius given by $\sqrt{D_{vr}^2 (R_{vt}^2 + h_v^2)^{\alpha_{vr}} - h_r^2}$. Then, we substitute R_{vt} from (20) in the area and use the Binomial expansion i.e., $(x+y)^\alpha = x^\alpha + \alpha x^{\alpha-1}y + \mathcal{O}(y)$, $y \ll x$, to obtain the required area for case 1. For case 2, we simply obtain the required area by calculating the area of the circle with radius $\sqrt{D_{vr}^2 (R_{vt}^2 + h_v^2)^{\alpha_{vr}} - h_r^2}$. For case 3, we use the formula for the area of intersection between two circles, which results in (39), where $\varrho(a, b, c)$ represents the area of the intersection of two circles with radii a and b with their centers separated by c and is given in (40). Finally, the mathematical manipulation of (39) leads to the area given in (25).

B. Proof of Lemma 2

Since there exists an overlap between $\mathcal{B}(u(0), R_k)$ and $\mathcal{B}(u(T), R_{kt})$, the required area can be calculated in the same way as in Case 3 of \mathcal{A}_{vr} and by considering $\alpha_{vr} = 1$, $D_{vr} = 1$, and $h_v = h_r$.

C. Proof of Lemma 3

Using the steps shown in [36, Section IV.B.], we can write the area $|\mathcal{A}_{rv}(R_r, v, T, \theta, D_{rv}, \alpha_{rv})|$ as given in (41), where $|\mathcal{B}(\cdot, \cdot) \setminus \mathcal{B}(\cdot, \cdot)|$ is given in (28). Using the Riemann integral, and letting $\frac{t}{T} = g$ in (41) with some mathematical manipulation lead to the area shown in (29).

REFERENCES

- [1] Huawei Technologies Co. Ltd., "5G-Oriented indoor digitalization solution," *White paper*, 2017, available at http://www-file.huawei.com/-/media/corporate/pdf/mbb/5g_oriented_indoor_digitalization_solution_white_paper_en.pdf.
- [2] Z. Zeng, M. D. Soltani, Y. Wang, X. Wu, and H. Haas, "Realistic indoor hybrid wifi and ofdma-based lifi networks," *IEEE Transactions on Communications*, vol. 68, no. 5, pp. 2978–2991, 2020.
- [3] Y. Wang and H. Haas, "Dynamic load balancing with handover in hybrid Li-Fi and Wi-Fi networks," *IEEE Journal of Lightwave Technology*, vol. 33, no. 22, pp. 4671–4682, 2015.
- [4] M. B. Rahaim and T. D. Little, "Toward practical integration of dual-use VLC within 5G networks," *IEEE Wireless Communications*, vol. 22, no. 4, pp. 97–103, 2015.
- [5] D. A. Basnayaka and H. Haas, "Hybrid RF and VLC systems: Improving user data rate performance of VLC systems," in *IEEE 81st Vehicular Technology Conference (VTC Spring)*, 2015, pp. 1–5.
- [6] H. Abuella, M. Elamassie, M. Uysal, Z. Xu, E. Serpedin, K. A. Qaraqe, and S. Ekin, "Hybrid RF/VLC systems: A comprehensive survey on network topologies, performance analyses, applications, and future directions," *arXiv preprint arXiv:2007.02466*, 2020.
- [7] Case studies archive - purelifi. Accessed: 2021-09-02. [Online]. Available: <https://purelifi.com/case-studies/>
- [8] M. Kashef, M. Ismail, M. Abdallah, K. A. Qaraqe, and E. Serpedin, "Energy efficient resource allocation for mixed RF/VLC heterogeneous wireless networks," *IEEE Journal on Selected Areas in Communications*, vol. 34, no. 4, pp. 883–893, 2016.
- [9] M. Kashef, M. Abdallah, and N. Al-Dhahir, "Transmit power optimization for a hybrid PLC/VLC/RF communication system," *IEEE Transactions on Green Communications and Networking*, vol. 2, no. 1, pp. 234–245, 2017.
- [10] H. Tabassum and E. Hossain, "Coverage and rate analysis for co-existing RF/VLC downlink cellular networks," *IEEE Transactions on Wireless Communications*, vol. 17, no. 4, pp. 2588–2601, 2018.

$$|\mathcal{A}_{\text{vr}}(R_{\text{v}}, v, T, \theta, D_{\text{vr}}, \alpha_{\text{vr}})| = \pi \left(D_{\text{vr}}^2 (R_{\text{v}}^2 + h_{\text{v}}^2)^{\alpha_{\text{vr}}} + \frac{\alpha_{\text{vr}} D_{\text{vr}}^2 (s^2 - 2R_{\text{v}}s \cos(\theta))}{(R_{\text{v}}^2 + h_{\text{v}}^2)^{1-\alpha_{\text{vr}}}} - h_{\text{r}}^2 \right) + \pi \left(D_{\text{vr}}^2 (R_{\text{v}}^2 + h_{\text{v}}^2)^{\alpha_{\text{vr}}} - h_{\text{r}}^2 \right) - \varrho \left(\pi (D_{\text{vr}}^2 (R_{\text{v}_t}^2 + h_{\text{v}}^2)^{\alpha_{\text{vr}}} - h_{\text{r}}^2), \pi (D_{\text{vr}}^2 (R_{\text{v}}^2 + h_{\text{v}}^2)^{\alpha_{\text{vr}}} - h_{\text{r}}^2), s \right) \quad (39)$$

$$\varrho(a, b, c) = a^2 \arccos \left(\frac{s^2 + a^2 - b^2}{2sa} \right) + b^2 \arccos \left(\frac{s^2 + b^2 - a^2}{2sb} \right) - \frac{1}{2} \sqrt{(-s + a + b)(s + a - b)(s - a + b)(s + a + b)} \quad (40)$$

$$|\mathcal{A}_{\text{rv}}(R_{\text{r}}, v, T, \theta, D_{\text{rv}}, \alpha_{\text{rv}})| = \pi (D_{\text{rv}}^2 (R_{\text{r}_t}^2 + h_{\text{r}}^2)^{\alpha_{\text{rv}}} - h_{\text{v}}^2) + \lim_{dt \rightarrow 0} \sum_0^{\frac{T}{dt} - 1} \left| \mathcal{B} \left(u(t), \sqrt{D_{\text{rv}}^2 (R_{\text{r}_t}^2 + h_{\text{r}}^2)^{\alpha_{\text{rv}}} - h_{\text{v}}^2} \right) \setminus \mathcal{B} \left(u(t + dt), \sqrt{D_{\text{rv}}^2 (R_{\text{r}_{t+dt}}^2 + h_{\text{r}}^2)^{\alpha_{\text{rv}}} - h_{\text{v}}^2} \right) \right| \quad (41)$$

-
- [11] J. Kong, M. Ismail, E. Serpedin, and K. A. Qaraqe, "Energy efficient optimization of base station intensities for hybrid RF/VLC networks," *IEEE Transactions on Wireless Communications*, vol. 18, no. 8, pp. 4171–4183, 2019.
- [12] H. Yang, A. Alphones, W.-D. Zhong, C. Chen, and X. Xie, "Learning-based energy-efficient resource management by heterogeneous RF/VLC for ultra-reliable low-latency industrial IoT networks," *IEEE Transactions on Industrial Informatics*, vol. 16, no. 8, pp. 5565–5576, 2019.
- [13] V. K. Papanikolaou, P. D. Diamantoulakis, P. C. Sofotasios, S. Muhaidat, and G. K. Karagiannidis, "On optimal resource allocation for hybrid VLC/RF networks with common backhaul," *IEEE Transactions on Cognitive Communications and Networking*, vol. 6, no. 1, pp. 352–365, 2020.
- [14] I. W. G. Da Silva, D. P. M. Osorio, E. E. B. Olivo, I. Ahmed, and M. Katz, "Secure hybrid RF/VLC under statistical queuing constraints," in *IEEE 17th International Symposium on Wireless Communication Systems (ISWCS)*, 2021, pp. 1–6.
- [15] H. Tabassum, M. Salehi, and E. Hossain, "Fundamentals of mobility-aware performance characterization of cellular networks: A tutorial," *IEEE Communications Surveys & Tutorials*, vol. 21, no. 3, pp. 2288–2308, 2019.
- [16] X. Lin, R. K. Ganti, P. J. Fleming, and J. G. Andrews, "Towards understanding the fundamentals of mobility in cellular networks," *IEEE Trans. Wireless Commun.*, vol. 12, no. 4, pp. 1686–1698, 2013.
- [17] F. Zhao, H. Tian, G. Nie, and H. Wu, "Received signal strength prediction based multi-connectivity handover scheme for ultra-dense networks," in *24th Asia-Pacific Conference on Communications (APCC)*, 2018, pp. 233–238.
- [18] X. Wu and H. Haas, "Handover skipping for lifi," *IEEE Access*, vol. 7, pp. 38 369–38 378, 2019.
- [19] M. Tayyab, X. Gelabert, and R. Jäntti, "A simulation study on handover in LTE ultra-small cell deployment: A 5G challenge," in *IEEE 2nd 5G World Forum (5GWF)*, 2019, pp. 388–392.
- [20] M. Tayyab, G. P. Koudouridis, X. Gelabert, and R. Jäntti, "Receiver power consumption during handover in LTE," in *2019 IEEE 2nd 5G World Forum (5GWF)*, 2019, pp. 74–79.
- [21] X. Wu and D. O'Brien, "A novel handover scheme for hybrid LiFi and WiFi networks," in *ICC 2020 - 2020 IEEE International Conference on Communications (ICC)*, 2020, pp. 1–5.
- [22] S. Sadr and R. Adve, "Handoff rate and coverage analysis in multi-tier heterogeneous networks," *IEEE Trans. Wireless Commun.*, vol. 14, no. 5, pp. 2626 – 2638, 2015.
- [23] M. Alhabo, L. Zhang, and N. Nawaz, "A trade-off between unnecessary handover and handover failure for heterogeneous networks," in *23th European Wireless Conference*, 2017, pp. 1–6.
- [24] W. Bao and B. Liang, "Stochastic geometric analysis of user mobility in heterogeneous wireless networks," *IEEE J. Sel. Areas Commun.*, vol. 33, no. 10, pp. 2212–2225, 2015.
- [25] S.-Y. Hsueh and K.-H. Liu, "An equivalent analysis for handoff probability in heterogeneous cellular networks," *IEEE Communications Letters*, vol. 21, no. 6, pp. 1405–1408, 2017.
- [26] Y. Ren, Y. Li, and C. Qi, "Handover rate analysis for k-tier heterogeneous cellular networks with general path-loss exponents," *IEEE Communications Letters*, vol. 21, no. 8, pp. 1863–1866, 2017.
- [27] R. Arshad, H. ElSawy, L. Lampe, and M. J. Hossain, "Handover rate characterization in 3D ultra-dense heterogeneous networks," *IEEE Transactions on Vehicular Technology*, vol. 68, no. 10, pp. 10 340–10 345, 2019.
- [28] M. T. Hossain and H. Tabassum, "Mobility-aware performance in hybrid RF and Terahertz wireless networks," *IEEE Transactions on Communications*, 2021.
- [29] H. Zhang, W. Ma, W. Li, W. Zheng, X. Wen, and C. Jiang, "Signalling cost evaluation of handover management schemes in LTE-advanced femtocell," in *IEEE 73rd Vehicular Technology Conference (VTC Spring)*, 2011, pp. 1–5.
- [30] H. Zhang, W. Zheng, X. Wen, and C. Jiang, "Signalling overhead evaluation of HeNB mobility enhanced schemes in 3GPP LTE-Advanced," in *IEEE 73rd Vehicular Technology Conference (VTC Spring)*, 2011, pp. 1–5.
- [31] M. Z. Chowdhury and Y. M. Jang, "Handover management in high-dense femtocellular networks," *EURASIP Journal on Wireless Communications and Networking*, no. 1, pp. 1–21, 2013.
- [32] R. Arshad, H. ElSawy, S. Sorour, T. Y. Al-Naffouri, and M.-S. Alouini, "Velocity-aware handover management in two-tier cellular networks," *IEEE Trans. Wireless Commun.*, vol. 16, no. 3, pp. 1851–1867, 2017.
- [33] —, "Handover management in 5G and beyond: A topology aware skipping approach," *IEEE Access*, vol. 4, pp. 9073–9081, 2016.
- [34] S. Shin, U. Lee, F. Dressler, and H. Yoon, "Analysis of cell sojourn time in heterogeneous networks with small cells," *IEEE Communications Letters*, vol. 20, no. 4, pp. 788–791, 2016.
- [35] X. Xu, Z. Sun, X. Dai, T. Svensson, and X. Tao, "Modeling and analyzing the cross-tier handover in heterogeneous networks," *IEEE Transactions on Wireless Communications*, vol. 16, no. 12, pp. 7859–7869, 2017.
- [36] M. Salehi and E. Hossain, "Stochastic geometry analysis of sojourn time in multi-tier cellular networks," *IEEE Transactions on Wireless Communications*, vol. 20, no. 3, pp. 1816–1830, 2020.
- [37] M. D. Soltani, H. Kazemi, M. Safari, and H. Haas, "Handover modeling for indoor Li-Fi cellular networks: The effects of receiver mobility and rotation," in *IEEE Wireless Communications and Networking Conference (WCNC)*, 2017, pp. 1–6.
- [38] A. M. Vegni and T. D. Little, "Handover in VLC systems with cooperating mobile devices," in *IEEE International conference on computing, networking and communications (ICNC)*, 2012, pp. 126–130.
- [39] E. Dinc, O. Ergul, and O. B. Akan, "Soft handover in OFDMA based visible light communication networks," in *IEEE 82nd Vehicular Technology Conference (VTC2015-Fall)*, 2015, pp. 1–5.
- [40] M. S. Demir, F. Miramirkhani, and M. Uysal, "Handover in VLC networks with coordinated multipoint transmission," in *IEEE International Black Sea Conference on Communications and Networking (BlackSeaCom)*, 2017, pp. 1–5.
- [41] M. D. Soltani, Z. Zeng, H. Kazemi, C. Chen, H. Haas, and M. Safari, "A study of sojourn time for indoor LiFi cellular networks," in *IEEE*

- 30th Annual International Symposium on Personal, Indoor and Mobile Radio Communications (PIMRC), 2019, pp. 1–6.
- [42] A. B. Ozyurt and W. O. Popoola, "Mobility management in multi-tier lifi networks," *Journal of Optical Communications and Networking*, vol. 13, no. 9, pp. 204–213, 2021.
- [43] J. Sanusi, S. Idris, A. M. Aibinu, S. Adeshina, and A. N. Obadiah, "Handover in hybrid LiFi and WiFi networks," in *IEEE 15th International Conference on Electronics, Computer and Computation (ICECCO)*, 2019, pp. 1–6.
- [44] R. Arshad and L. Lampe, "Stochastic geometry analysis of user mobility in RF/VLC hybrid networks," *IEEE Transactions on Wireless Communications*, vol. 20, no. 11, pp. 7404–7419, 2021.
- [45] A. L. E. Corral-Ruiz, F. A. Cruz-Pérez, G. Hernández-Valdez, and A. Ek-sim, "Cell dwell time and channel holding time relationship in mobile cellular networks," in *Wireless Communications and Networks—Recent Advances*. InTech, 2012, pp. 357–378.
- [46] Evolved Universal Terrestrial Radio Access (E-UTRA), "Mobility enhancements in heterogeneous networks," *3GPP TR 36.839, Tech. Rep.*, 2012.
- [47] J. G. Andrews, F. Baccelli, and R. K. Ganti, "A tractable approach to coverage and rate in cellular networks," *IEEE Trans. Commun.*, vol. 59, no. 11, pp. 3122–3134, 2011.
- [48] Y. Hmamouche, M. Benjillali, S. Saoudi, H. Yanikomeroglu, and M. Di Renzo, "New trends in stochastic geometry for wireless networks: A tutorial and survey," *Proceedings of the IEEE*, 2021.
- [49] C. Chen, D. Basnayaka, and H. Haas, "Downlink SINR statistics in OFDM-based optical attocell networks with a Poisson point process network model," in *IEEE Global Communications Conference (GLOBE-COM)*, 2015, pp. 1–6.
- [50] Chiu *et al.*, *Stochastic Geometry and its Applications*. John Wiley & Sons, 2013.
- [51] A. K. Gupta and A. Banerjee, "On the spatial performance of users in indoor VLC networks with multiple reflections," in *IEEE International Conference on Signal Processing and Communications (SPCOM)*, 2018, pp. 512–516.
- [52] H.-S. Jo, Y. J. Sang, P. Xia, and J. G. Andrews, "Heterogeneous cellular networks with flexible cell association: A comprehensive downlink SINR analysis," *IEEE Trans. Wireless Commun.*, vol. 11, no. 10, pp. 3484–3495, 2012.
- [53] P. F. Ash and E. D. Bolker, "Generalized dirichlet tessellations," *Geometriae Dedicata*, vol. 20, no. 2, pp. 209–243, 1986.
- [54] J. Meinilä, P. Kyösti, T. Jämsä, and L. Hentilä, "Winner II channel models," *Radio Technologies and Concepts for IMT-Advanced*, pp. 39–92, 2009.
- [55] C. Chen, D. A. Basnayaka, and H. Haas, "Downlink performance of optical attocell networks," *IEEE Journal of Lightwave Technology*, vol. 34, no. 1, pp. 137–156, 2015.
- [56] J. Armstrong and B. J. Schmidt, "Comparison of asymmetrically clipped optical OFDM and DC-biased optical OFDM in AWGN," *IEEE Communications Letters*, vol. 12, no. 5, pp. 343–345, 2008.
- [57] J. M. Kahn and J. R. Barry, "Wireless infrared communications," *Proceedings of the IEEE*, vol. 85, no. 2, pp. 265–298, 1997.
- [58] M. Ding and D. L. Pérez, "Please lower small cell antenna heights in 5G," in *IEEE Global Communications Conference (GLOBECOM)*, Washington, DC, 2016, pp. 1–6.
- [59] L. Heinrich, "Contact and chord length distribution of a stationary Voronoi tessellation," *Advances in Applied Probability*, vol. 30, no. 3, pp. 603–618, 1998.
- [60] H. ElSawy, E. Hossain, and M. Haenggi, "Stochastic geometry for modeling, analysis, and design of multi-tier and cognitive cellular wireless networks: A survey," *IEEE Communications Surveys & Tutorials*, vol. 15, no. 3, pp. 996–1019, 2013.
- [61] M. Haenggi, *Stochastic geometry for wireless networks*. Cambridge University Press, 2012.
- [62] Evolved Universal Terrestrial Radio Access (E-UTRA), "LTE protocol specification," *3GPP TS 36.331, Tech. Rep.*, 2013.
- [63] T. Liu, S. Zhou, and Z. Niu, "Mobility-aware coded-caching scheme for small cell network," in *IEEE International Conference on Communications (ICC)*, 2017, pp. 1–6.
- [64] M. Afzalan and F. Jazizadeh, "Indoor positioning based on visible light communication: A performance-based survey of real-world prototypes," *ACM Computing Surveys (CSUR)*, vol. 52, no. 2, pp. 1–36, 2019.